Arch. Metall. Mater. **70** (2025), 3, 1085-1088

DOI: https://doi.org/10.24425/amm.2025.154447

JOON PHIL CHOI[1*], YONGRAE KIM[1], DONGWOON SHIN[1], MIN-KYO JUNG[1], PIL-HO LEE[1], SEUNG KI MOON[2], HAINING ZHANG[3*]

COMPARISON AND IDENTIFICATION OF OPTIMAL MACHINE LEARNING MODEL FOR RAPID PROCESS MODELING OF AEROSOL JET PRINTING TECHNOLOGY

Aerosol Jet Printing (AJP) offers high resolution and flexible working distances, making it a promising technology for the customization of complex electronic devices. However, devices fabricated through the AJP process often suffer from reduced electrical performance due to limited control over printed line width, which constrains its applicability in advanced electronic manufacturing. Consequently, achieving high precision in line width control is of paramount importance for optimizing AJP technology. In this research, a machine learning framework is proposed to enable rapid modeling of printed line width. The framework considers sheath gas flow rate, carrier gas flow rate, and print speed as input variables, with line width as the target output. Three representative machine learning algorithms – support vector regression, artificial neural networks, and XGBoost – were employed to develop predictive models. The modeling performance of these algorithms was systematically compared using four conventional evaluation metrics. Ultimately, the optimal machine learning model identified through this process was selected for the rapid modeling of printed line width in the AJP process.

Keywords: Machine learning; Process modeling; Printed line width; Aerosol jet 3D printing; Optimal model identification

1. Introduction

With the rising demand for rapid prototyping and customizable micro-electronic devices, direct-write (DW) technology is emerging as a crucial solution in the electronic manufacturing industry [1]. Among the various DW techniques, aerosol jet printing (AJP) is particularly noteworthy due to its high resolution (approximately 10 μm) and versatile working distance (2-5 mm) [2]. These characteristics position AJP as an effective method for the precise fabrication of complex electrical devices, including fully additively manufactured passive components, compact printed circuit boards, and advanced electromagnetic devices [3]. While AJP technology offers numerous advantages, micro-electronic devices produced using AJP often exhibit suboptimal electrical performance due to issues related to line geometry, such as line edge roughness and overspray. However, a more critical concern lies in the limited precision of line width control, which can lead to overlapping circuits or gaps between closely spaced tracks [4]. This limitation poses a significant barrier to the widespread adoption of AJP technology in advanced electronic manufacturing. Therefore, achieving precise control over line width is crucial for the success of AJP technology.

Currently, many designers rely on a trial-and-error approach to determine the appropriate process parameters to maintain the geometric accuracy of printed microelectronics. This method lacks a systematic and intelligent framework for optimizing the process parameters of AJP, resulting in inefficiency and higher costs [5,6]. There is a clear need for a modeling and optimization framework that can quantitatively evaluate the effects of process parameters on printed line characteristics and determine universally optimal parameters. To address this issue, various simplified analytical models have been developed to study the influence of critical process parameters on printed line outcomes. However, these models primarily identify broad trends due to system variability and the complexity of the AJP process. Additionally, several computational fluid dynamics (CFD) models have been developed to investigate aerosol transport and deposition mechanisms in the AJP process. Although 2D and 3D CFD models theoretically analyze the impact of key process parameters, their practicality for fast process modeling and optimization

[1] DEPARTMENT OF 3D PRINTING, KOREA INSTITUTE OF MACHINERY & MATERIALS, DAEJEON, REPUBLIC OF KOREA
[2] SCHOOL OF MECHANICAL AND AEROSPACE ENGINEERING, NANYANG TECHNOLOGICAL UNIVERSITY, SINGAPORE, SINGAPORE
[3] SCHOOL OF INFORMATION ENGINEERING, SUZHOU UNIVERSITY, SUZHOU, CHINA

* Corresponding authors: jpchoi@kimm.re.kr; m160034@e.ntu.edu.sg

is limited by computational resource requirements, which in turn restricts their ability to enhance control over printed line width during fabrication [7,8].

This research explores the application of machine learning techniques for rapid process modeling in AJP, aimed at improving control over printed line width by analyzing the relationships between process parameters and output. Machine learning is preferred for its efficiency and minimal prerequisite knowledge, and it stands out from conventional theoretical modeling approaches [9-11]. Given the novelty of AJP within DW technologies and the limited number of meta-modeling studies available, this research systematically evaluates machine learning approaches for modeling the printed line width in AJP. The study primarily focuses on the effects of sheath gas flow rate (SHGFR), carrier gas flow rate (CGFR), and print speed on line width, demonstrating that machine learning provides superior efficiency and accuracy in modeling compared to traditional methods, thereby facilitating precise control over line width during the printing process.

2. Experimental

Fig. 1(a) illustrates the operational stages of AJP technology. Initially, liquid ink is atomized into an aerosol consisting of 2-5 μm droplets using either an ultrasonic (1-10 mPa·s) or pneumatic (10-1000 mPa·s) atomizer. The aerosol is then transported to the printhead by a nitrogen carrier gas. Subsequently, an annular nitrogen sheath gas flow collimates and accelerates the aerosol, which is ejected from the nozzle tip onto a moving substrate, forming 2D or 3D structures with a resolution of approximately 10 μm [12-14]. In this study, Clariant® silver nanoparticle ink was employed to create conductive silver patterns on polyimide substrates, with the ink vial temperature maintained at 20°C. The specifics of the experimental setup and workspace are detailed in TABLE 1, where sccm represents standard cubic centimeters per minute.

Although extensive datasets for process modeling can improve the accuracy of AJP, the limitations in the precision of process parameters and system drift during printing restrict the number of feasible experimental points within the design space. As a result, it is crucial to adopt a machine learning approach that is optimized for smaller datasets to expedite the process of AJP optimization [15-17]. In this study, Latin hypercube sampling (LHS) was utilized for experimental design to ensure comprehensive coverage of the design space and to rigorously examine the interactions between various process parameters and the printed line attributes. Initially, 95 experimental points were generated using LHS, as shown in Fig. 1(b). At each experimental point, a single 5 mm line was printed on the substrate, and the process was repeated three times under identical conditions to ensure consistency.

Fig. 2(a) outlines the characteristics of the printed lines, such as line width, edge roughness, and overspray. As the conductivity of these lines is not significantly influenced by isolated overspray spots, the initial microscope images of the line samples were processed using a denoising algorithm, as shown in Fig. 2(b) and (c). Following this, an image processing technique, depicted in Fig. 2(e), was employed to extract the features of the printed lines for detailed analysis. Furthermore, Fig. 2(d) illustrates the calculation of the average line width, where w_i represents the width of the i^{th} column.

$$\bar{w} = \frac{1}{N}\sum_{i=1}^{N} w_i \tag{1}$$

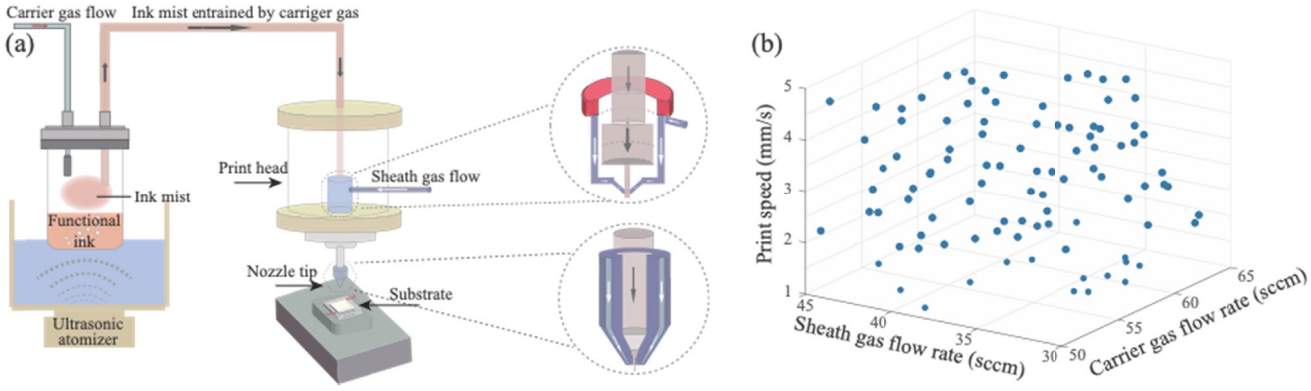

Fig. 1. (a) Illustration of aerosol jet printing working principles using an ultrasonic atomizer, (b) experimental design based on LHS

TABLE 1

Experimental setup of the AJP process

Working conditions				Control parameters		
Working distance (mm)	**Tip diameter (μm)**	**Ink temperature (°C)**	**Atomization current (mA)**	**SHGFR (sccm)**	**CGFR (sccm)**	**Print speed (mm/s)**
3	150	20	0.45	[40, 60]	[25, 40]	[1, 5]

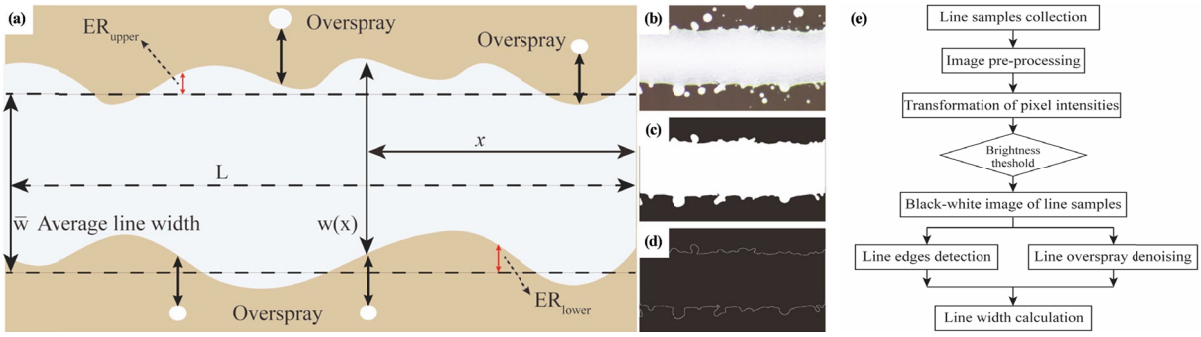

Fig. 2. Characteristics of printed line samples. (a) Outline of line features, (b) initial image of a line sample, (c) denoised image of a line sample, (d) features extracted from a line sample. (e) Image processing flow chart for printed line features extraction

3. Results and discussion

In this study, we selected Support Vector Regression (SVR), Backpropagation Neural Networks (BPNNs), and XGBoost as representative models based on their complementary strengths and proven success in regression tasks. SVR was chosen for its ability to generalize well with limited data and its robustness to high-dimensional inputs via kernel functions. BPNNs were included due to their capability to model complex nonlinear relationships through layered architectures and gradient-based learning. XGBoost was selected for its high performance in structured data regression, benefiting from ensemble learning, regularization, and efficient computation. These models represent three distinct paradigms – kernel-based, neural-based, and tree-based allowing a comprehensive evaluation of regression performance across different methodological frameworks.

In this study, the proportion of the test dataset varied from 10% to 40%, increasing in increments of 5%. To minimize the impact of random variations on the results, each dataset configuration was evaluated 30 times, and the average R value was used as the performance metric. Fig. 3 demonstrates the effects of different dataset splits on performance, with respect to the SVR, XGBoost, and BPNNs models. It was noted that altering the size of the training dataset had a negligible impact on performance, with the R value remaining relatively stable around 0.95. Conversely, the highest R value was observed when the test dataset size was 20% with respect to different models; beyond this point, the R value tended to decline as the test dataset size increased to 35%. Based on these findings, both the SVR model and similar models, such as BPNNs and XGBoost, performed best with a 20% test dataset. Therefore, an 80% training and 20% testing dataset split was established as the optimal ratio for this research.

Fig. 4 illustrates the correlations between printed line width and two process parameters, with the third process parameter in each subplot set to its average value. The modeling results reveal the complex interactions among different process parameters. Fig. 4 shows that, according to the continuity equation, the

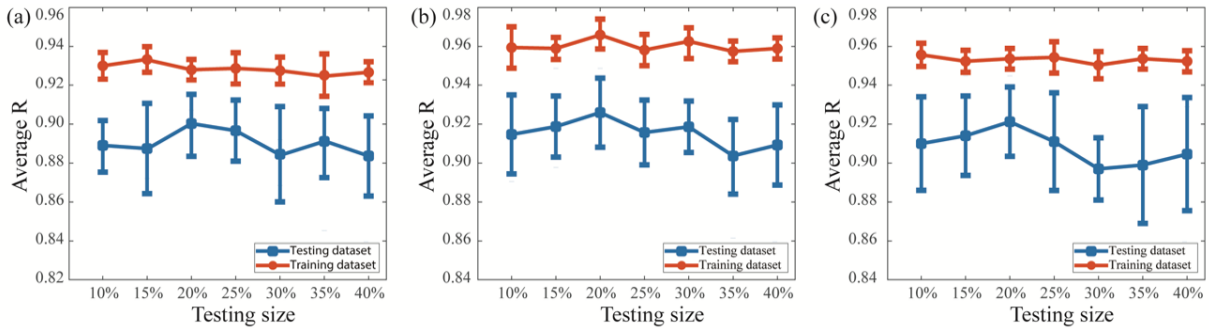

Fig. 3. The impact of the data size proportion on modeling performance of (a) BPNNs, (b) XGBoost and (c) SVR

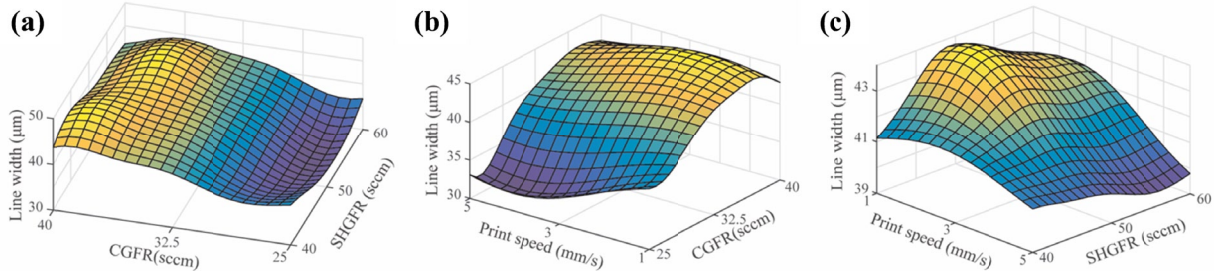

Fig. 4. The correlations between the printed line width and the process parameters based on XGBoost model

carrier gas flow rate (CGFR) positively affects the line width, whereas the sheath gas flow rate (SHGFR) has an inverse effect. Additionally, due to the complex aerodynamics within the printhead, the interaction between CGFR, SHGFR, and print speed exerts a non-linear influence on the printed line width. This effect is primarily driven by the velocity and pressure buildup in the combination chamber, resulting from increased gas flow rates and print speed. Variations in the velocity and pressure fields affect the Saffman lift force and Stokes drag force acting on the aerosol droplets, which in turn influence their trajectory at the nozzle exit [18]. These aerodynamic effects are critical in determining the printed line width, as they alter the distribution and deposition of aerosol particles [19]. Understanding this relationship is essential for controlling how fine adjustments in print parameters translate into changes in the final printed features [20].

TABLE 2

Modeling performance of printed line width based on four classic evaluation indicators

Model	Training dataset				Testing dataset			
	RMSE	MAE	R	R^2	RMSE	MAE	R	R^2
SVR	2.79	2.91	0.95	0.94	4.16	3.53	0.92	0.86
BPNNs	3.15	3.69	0.93	0.91	5.27	4.25	0.91	0.83
XGBoost	2.19	1.96	0.96	0.95	3.59	3.16	0.93	0.89

The evaluation of the process models developed using SVR, BPNNS and XGBoost is presented in TABLE 2. Metrics such as R and R^2 were initially used to compare the models, revealing high values that indicate these models accurately represent the overall trends of the AJP process. Notably, of the three developed models, XGBoost exhibited the best performance, leveraging its flexible modeling approach, which proved more effective than both BPNNs and SVR. Further evaluation using Mean Absolute Error (MAE) and Root Mean Square Error (RMSE) supported these findings, as outlined in TABLE 2. The XGBoost model consistently reported lower MAE and RMSE values across both the training and testing datasets, demonstrating its superior predictive accuracy.

4. Conclusions

This study explores the use of machine learning techniques, specifically SVR, BPNNs, and XGBoost, to optimize line quality in the AJP process. The modeling results revealed that the optimal dataset split was 80% for training and 20% for testing, which provided the best performance. Additionally, XGBoost outperformed the other models in terms of predictive accuracy, as evidenced by lower RMSE and MAE values. Moreover, the analysis highlights significant interactions between key process parameters, such as carrier gas flow rate, sheath gas flow rate, and print speed, all of which influence the printed line width. These results provide a solid foundation for future work, which will aim to incorporate additional factors such as ink and substrate properties to further enhance print quality and process optimization.

Acknowledgments

This research was supported by the Basic Research Program funded by the Korea Institute of Machinery & Materials (KIMM) (No. NK255C) and the Technology Innovation Program funded by the Ministry of Trade, Industry & Energy (MOTIE, Korea) (No. RS-2024-00441774). This research was also supported by the Suzhou University (No. 2021BSK023, No. 2021XJPT51, No. 2019xjzdxk1, szxy2023jyjf84).

REFERENCES

[1] J. Bae, S. Jo, K.T. Kim, J. Powder Mater. **30**, 318 (2023).
[2] J. Chang, X. Zhang, T. Ge, J. Zhou, Org. Electron. **15**, 701 (2014).
[3] H.S. Kim, J.S. Kang, J.S. Park, H.T. Hahn, H.C. Jung, J.W Joung, Compos. Sci. Technol. **69**, 1256 (2009).
[4] J. Zikulnig, C. Hirschl, L. Rauter, M. Krivec, H. Lammer, F. Riemelmoser, A. Roshanghias, Flex. Print. Electron. **4**, 015008 (2019).
[5] R. Liu, H. Ding, J. Lin, F. Shen, Z. Cui, T. Zhang, Nanotechnology **23**, 505301 (2012).
[6] S. Vella, C.S. Smithson, K. Halfyard, E. Shen, M. Chrétien, Flex. Print. Electron. **4**, 045005 (2019).
[7] S.K. Eshkalak, A. Chinnappan, W. Jayathilaka, W.A.D.M. Jayathilaka, M. Khatibzadeh, E. Kowsari, S. Ramakrishna, Appl. Mater. Today. **9**, 372 (2017).
[8] D. Zhao, T. Liu, J.G. Park, M. Zhang, J.M. Chen, B. Wang, Microelectron. Eng. **96**, 71 (2012).
[9] B.Q. Wei, R. Vajtai, P.M. Ajayan, Appl. Phys. Lett. **79**, 1172 (2001).
[10] G.L. Goh, S. Agarwala, W.Y. Yeong, Adv. Mater. Interfaces **6**, 1801318 (2019).
[11] H. Zhang, S.K. Moon, ACS Appl. Mater. Interfaces **13**, 53323 (2021).
[12] M. Smith, Y.S. Choi, C. Boughey, S. Kar-Narayan, Flex. Print. Electron. **2**, 015004 (2017).
[13] H. Zhang, S.K. Moon, Int. J. of Precis. Eng. and Manuf-Green. Tech. **7**, 511 (2020).
[14] H. Zhang, J.P. Choi, S.K. Moon, T.H. Ngo, J. Mater. Process. Technol. **285**, 116779 (2020).
[15] R.R. Salary, J.P. Lombardi, M. Samie Tootooni, R. Donovan, P.K. Rao, P. Borgesen, M.D. Poliks, J. Manuf. Sci. Eng. **139**, 021015 (2017).
[16] H. Zhang, J.P. Choi, S.K. Moon, T.H. Ngo, Addit. Manuf. **33**, 101096 (2020).
[17] Y. Oh, D. Suh, Y. Kim, E. Lee, J.S. Mok, J. Choi, S. Baik, Nanotechnology **19**, 495602 (2008).
[18] S. Ramesh, C. Mahajan, S. Gerdes, A. Gaikwad, P. Rao, D.R. Cormier, I.V. Rivero, Addit. Manuf. **59**, 103090 (2022).
[19] Z. Liu, Y. Liu, L. He, L. Cui, N. Liang, J.P. Choi, H. Zhang, Int. J. Precis. Eng. Manuf.-Green Technol. **11**, 727 (2024).
[20] H. Zhang, J. Huang, X. Zhang, C.N. Wong, Addit. Manuf. **86**, 104208 (2024).